Inertially driven buckling and overturning of jets in a Hele-Shaw cell

Adriana I. Pesci, Martin A. Porter, and Raymond E. Goldstein

Department of Physics and Program in Applied Mathematics, University of Arizona, Tucson, Arizona 85721, USA

We study a fluid jet descending through stratified surroundings at low Reynolds number in Hele-Shaw flow. The jet buckles and overturns inside a conduit of entrained fluid which supports smooth or unstable traveling waves. A model of the recirculating flow within the conduit shows that buckling and waves arise from Kelvin-Helmholtz instabilities and quantitatively accounts for the main experimental observations. Beyond the onset of the instability, a damped, forced Burgers' equation obtained from corrections to Darcy's law for small Reynolds number governs the interface dynamics and supports singularities corresponding to the observed jet overturning and unstable waves.

Fluid flow between parallel plates, the geometry of Hele-Shaw cells, is often considered a quintessential low Reynolds number system [1]. Yet, in the laboratory it is straightforward to achieve a Reynolds number (Re) of order 1 with conventional fluids and relatively small plate spacings. This raises the interesting possibility of investigating inertial effects in a controlled manner by varying the fluid viscosity, cell geometry, and gravitational forcing. Indeed, some of these inertial effects have been studied, such as irreversibility [2] and instabilities in otherwise stable systems [3–5].

A classic example of an inertial instability is the buckling of fluid jets, whose long history starts from the work of Taylor [6] and continues more recently [7,8] with jets surrounded by air impacting on a surface. Variants of these phenomena have geophysical [9], astrophysical [10], and biological counterparts. Indeed, our primary motivation is the understanding of instabilities of descending jets of bacteria-rich fluid in bioconvecting suspensions [11]. We study a simplified model of that system suggested by Kessler: the dynamics of saline jets descending through a surrounding fluid with a linear salinity gradient. We find that these jets gradually decelerate and buckle (Fig. 1). Unlike those mentioned above, our system is dominated by viscous shear. This case has been studied theoretically [12] for jets surrounded by a fluid of uniform density. As a first approach to understanding the full three-dimensional jet [13] we study here the analogous effect in Hele-Shaw flow. As a function of the flow rate of the jet, we find experimentally a supercritical bifurcation in which the amplitude of the buckled jet is the order parameter, and its oscillation frequency is finite at onset. This buckling occurs within an entrained *conduit* of fresh water, a consequence of the surrounding density gradient. The existence and characteristics of this conduit constitutes a nontrivial free-boundary problem which has not yet been solved fully. Instead, we derive an approximate conduit shape by proposing its existence and solving the Stokes equations under simplifying assumptions and constraints. A key consequence of this analysis is a fluid velocity profile consistent with the development of linear Kelvin-Helmholtz instabilities of the jet and the conduit boundaries. We show that this quantitatively explains the major observed features of the buckling. To describe the nonlinear behavior of the jet within the conduit, specifically its secondary instabilities

(Figs. 2 and 3), we discuss a generalization of Darcy's law to include weak inertia, expressing the results through coupled partial differential equations for the vortex sheet strength γ at the interface between the two fluids and the position of the interface itself, by analogy to the approach for the inviscid case of Pugh and Shelley [14].

The only significant optical distinction between the jet and surrounding fluid is a small difference in their indices of
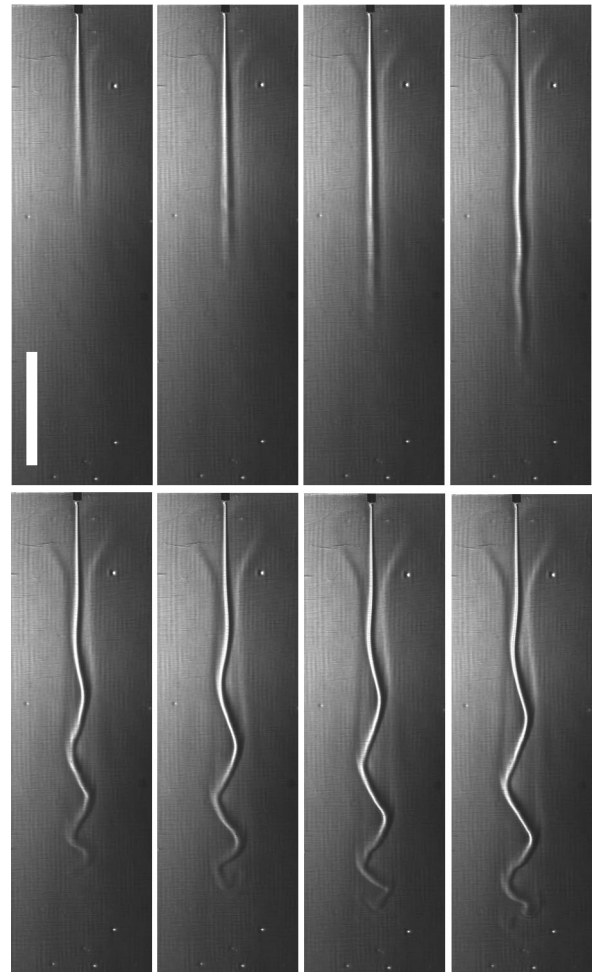

FIG. 1. A 1 M/l jet descending into a gradient 0.04 M/(l cm) at velocities from 0.02 to 0.18 cm/s. Scale is 1 cm.
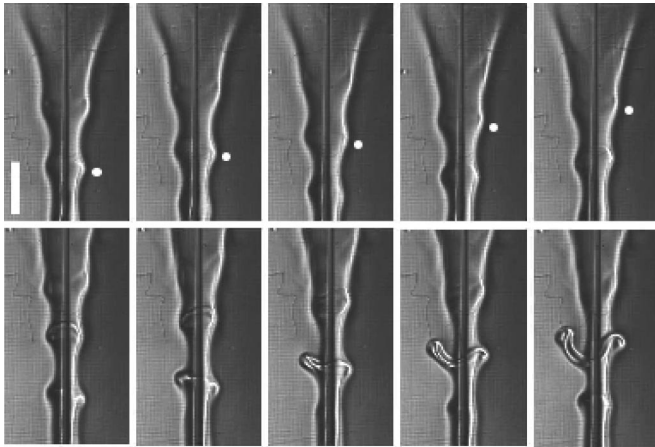
FIG. 2. Waves at the conduit edge just below the nozzle, at a velocity $u=1.5$ cm/s$\gg u_c$, for the same jet molarity and gradient as in Fig. 1. The buckled region of the jet further down is not shown. Upper sequence—growth and subsequent decay (white circles); lower sequence—unstable growth. Images are 0.8 s apart; scale bar is 0.5 cm.

refraction. This feature makes the flow patterns observable best with a technique such as Schlieren imaging that is sensitive to gradients of refractive index. Our Schlieren system is in the standard "Z" configuration, with video images acquired from a digital charge-coupled device (CCD) camera under computer control [15]. The Hele-Shaw cell consists of two 30×30 cm polycarbonate sheets 12.7 mm thick, separated by a rubber gasket 3 mm thick. A needle with interior diameter of 0.05 cm (25 ga) at the top of the chamber is the entry point for the jet. Two needles inserted through ports (Instech Labs, PMINP-SIL-C35) mounted at the bottom of one of the plates are the entry points for the fluid surround. The jet is forced into the chamber with a syringe pump driving a gas-tight glass syringe. We shall use the average fluid velocity u at the needle associated with the pump-controlled flux as our control parameter. Velocities range from 0.02 to 1 cm/s. Solutions were made from reverse osmosis purified
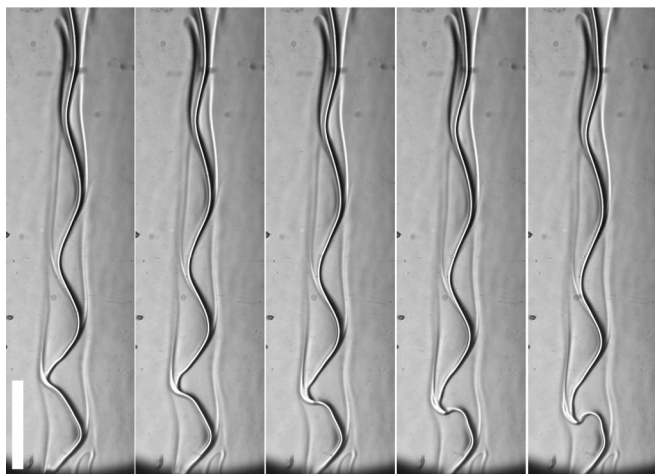

FIG. 3. Buckling and overturning of a jet descending through a gradient, with parameters as in Fig. 1 and $u=0.3$ cm/s. Images are 0.66s apart; scale bar is 1 cm.

water and reagent-grade NaCl (Sigma), with a diffusion constant of $D=1.5\times10^{-5}$ cm^2/s [16]. Linear salinity gradients were produced by a variant of the well-known "two-bucket" method in which the fluid flow was controlled by peristaltic pumps. A typical gradient is 0.04 M/(1 cm) (0.024 g/cm^4) and has a concentration of 1.0 M/l at the bottom and 0 M/l at the top, with a maximum variation in the index of refraction of about 0.01 [16]. Jet concentrations of 1–2 M/l were investigated. For the above values of u, the Reynolds number of the jet (naturally calculated as uw/ν), where w the jet diameter and $\nu=0.01$ cm^2/s the kinematic viscosity of water, is in the range of 0.03–3.

As shown in Fig. 1, at low flow velocities the jet is straight, disappearing by diffusion at a termination length ℓ which increases with flow rate. For each gradient and jet molarity there is a critical velocity u_c above which the jet buckles and ℓ grows more slowly. The density of the jet in this figure equals the fluid density at the *bottom* of the chamber, so its termination at a small fraction of the depth of the gradient indicates that it loses salt through diffusion. Salt diffusion across w occurs on a time scale $t_D\sim w^2/D$ ~170 s, while, at the lowest flow rates the advection time t_a for a fluid element to traverse the length $\ell\sim2$ cm is t_a $\sim\ell/u\sim100$ s. Clearly, there is sufficient time for appreciable diffusive broadening to occur, as seen in the figure.

At all flow rates we find that the jet, whether straight or buckled, is traveling inside a conduit whose edges can be clearly seen in Figs. 1–3. Near the nozzle the conduit flares upward away from the jet, narrows to a minimum somewhat below the nozzle, and then increases steadily downward. When the jet buckles, its amplitude maxima always approach the edges of the conduit as they travel downward. Observing the motion of tracer particles (10 μm hollow glass spheres, Potters Industries), we determined that the conduit consists of essentially fresh water viscously entrained from above by the jet to the point at which buoyancy drives it upward along the conduit edge. Evidence for recirculation within the conduit can clearly be seen at large flow rates, when wavelike excitations ("*blips*") (Fig. 2) travel up the edge [9].

Beyond the critical velocity we see a classical bifurcation scenario as mentioned earlier. This is shown in Fig. 4, where we have recorded the amplitude, frequency, and initial wavelength as a function of u for a particular gradient and jet density. The amplitude (measured for the wave farthest from the nozzle, where the conduit has saturated) and frequency data are consistent with a supercritical Hopf bifurcation. Over a wide range of flow rates beyond u_c the jet maintains its thickness as it descends, and its wavelength decreases. Beyond u_c and with increasing nozzle velocity the buckled jet amplitude either transiently grows and then decays toward the termination point or a secondary instability develops as the jet continues to grow and eventually overturns (Fig. 3). Because the density difference between the conduit and the surrounding gradient decreases with height, so that the fluid velocity at the conduit edge likewise decreases, a similar effect occurs with the blips: they either transiently grow and then decay or continue to grow and eventually form a separate plume (Fig. 2). The periodicity of these waves appears to coincide with the buckling frequency of the
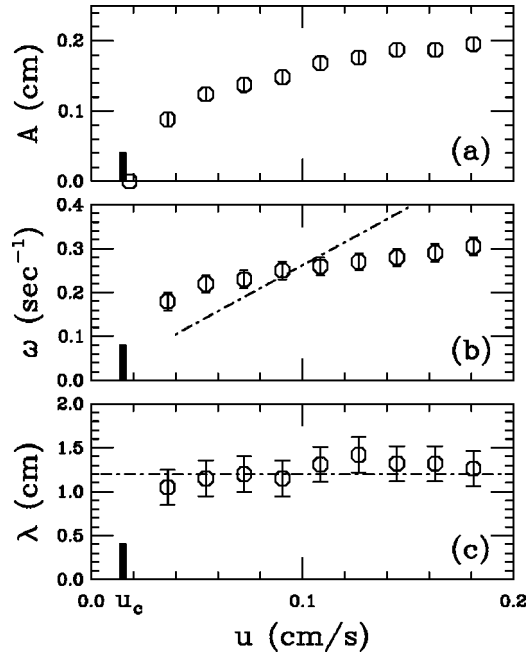
FIG. 4. Maximum buckling amplitude (a), frequency (b), and initial wavelength (c) versus flow rate for a gradient of 0.04 M/(l cm) and a 1.0 M/l jet. Critical velocity u_c and dashed lines in (b) and (c) are theoretical predictions.
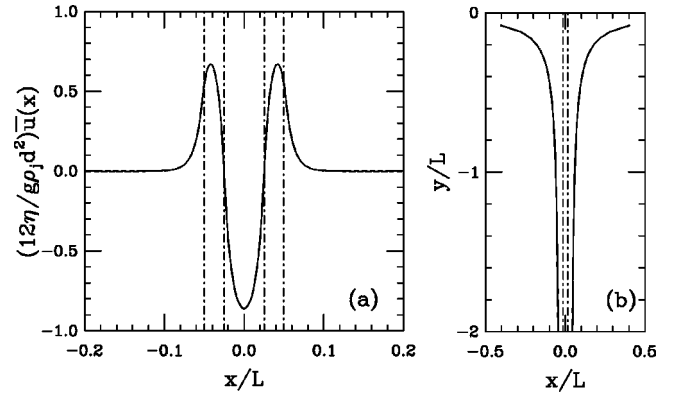

FIG. 5. Theoretical velocity profile (a) showing jet and conduit (inner and outer pairs of dashed lines) and interpolated conduit shape (b) on a larger scale, showing jet (dashed).

jet far below the region shown. There are corresponding "antiblips" on the jet itself that travel downward and may also grow so large as to detach.

A three-dimensional model of the conduit shape at low Reynolds number leads to a quantitative explanation of jet buckling as a Kelvin-Helmholtz instability. Since the conduit size varies on a scale large compared to its width, we study as a first approximation a *three-fluid* model consisting of a jet of density ρ_j and width w surrounded by an upward-flowing fresh-water conduit (density ρ_0 and width w_c), in turn surrounded by a denser outer fluid (ρ_s), all with uniform densities and only vertical velocities u. Fixing the three densities and the jet width, we determine numerically the single free parameter w_c by the simple hypothesis of zero total vertical flux. The shape of the conduit in the presence of a gradient is then deduced by taking these results and parametrically plotting the conduit width versus vertical density difference.

For rectangular channel geometry, with the piecewise constant density described above, we first solve $\eta \nabla^2 u = g\rho(x)$ using Green's function and then average u over the gap width to obtain $\bar{u}$, the reverse order of that used when applying Darcy's law. This yields a continuous velocity profile, such as that in Fig. 5(a), which corresponds to the experimental case in which the gap spacing d is comparable to the jet width. The associated conduit, shown in Fig. 5(b), displays the experimental feature of narrowing with depth, a consequence of the slower jet velocity and thus weaker viscous entrainment. Parallel to the jet-conduit interface are two flows in opposite directions, and this gives rise to a Kelvin-Helmholtz instability. The transition zone connecting the two flows has a finite width and can be shown to follow approximately the form $\tanh(\pi x/d)$; the transition zone width is set

by the Hele-Shaw gap. Using Drazin's results for the Kelvin-Helmholtz (KH) instability of this profile [17], we deduce that the most unstable mode of that instability will be at a wavelength of $4d \sim 1.2$ cm. As shown in Fig. 4(c) this is in good agreement with the experiments. If u and $\tilde{u}$ are the maximum jet and conduit velocities, respectively, then the propagation speed of the wave, $c = (u - \tilde{u})/2$, follows directly from a generalization of the KH stability analysis in Hele-Shaw flow [5]. Near the top of the chamber, $\tilde{u} \ll u$, as the conduit is much wider than the jet, so $c \sim u/2$, yielding a frequency $\omega \sim (\pi/4d)u$, also in good agreement with the data near onset [Fig. 4(b)]. The corresponding period of the KH wave is $8d/u$. When this time is shorter than the typical diffusion time t_D, the instability can occur. Equating these two time scales leads to a predicted critical velocity $u_c = 8Dd/w^2$. For the data shown, $u_c \sim 0.015$ cm/s, in good agreement with the observed value. An additional important feature of the velocity profile in Fig. 5 is an inflection point near the conduit edge, providing the source for a second KH instability, corresponding to the blips shown in Fig. 2.

A theory of the fully developed buckled jet is lacking. However, it is possible to gain insight into that nonlinear behavior and the onset of inertially driven secondary instabilities by extending leading-order inertial corrections to Darcy's law [3,5] to the vortex sheet representation for interface dynamics. Consider a Hele-Shaw cell of lateral dimensions $L \times L$, with plate spacing $d \ll L$, filled with fluids of common viscosity η. Assuming that there exists a characteristic velocity U, we define anisotropic rescalings $\tilde{\mathbf{u}} = U\mathbf{v}$, $t = (L/U)\tau$, $x' = x/L$, $y' = y/L$, and $z' = z/d$, where (x,y) are in-plane coordinates and z is perpendicular to the plates. Neglecting the component of $\mathbf{v}$ in the z direction, and introducing the rescalings into the Navier-Stokes equation, we obtain

$$\text{Re}\frac{d}{L}\left[\frac{\partial \mathbf{v}}{\partial \tau} + (\mathbf{v}\cdot\boldsymbol{\nabla}')\mathbf{v}\right] = -\frac{d^2}{U_0\eta L}\boldsymbol{\nabla}'p + \frac{\partial^2 \mathbf{v}}{\partial z'^2}, \quad (1)$$

where $\boldsymbol{\nabla}' = (\partial/\partial x')\hat{\mathbf{x}} + (\partial/\partial y')\hat{\mathbf{y}}$ and $\text{Re} = \rho U d/\eta$.

Expanding $\mathbf{v}$ in powers of Re as $\mathbf{v}=\mathbf{v}_0+\mathrm{Re}\ \mathbf{v}_1+O(\mathrm{Re}^2)$, it is then a straightforward exercise to substitute into Eq. (1), solve for $\mathbf{v}_0$ and $\mathbf{v}_1$ subject to the usual stick boundary conditions at the plates, average over the z coordinate, and then undo the original rescalings to obtain the averaged velocity $\mathbf{u}$ up to first order in Re. The velocity field can be recast in terms of the vortex sheet strength γ at the interface(s) Γ between the two fluids, where $\gamma=\hat{\mathbf{t}}\cdot(\mathbf{u}_1-\mathbf{u}_2)|_\Gamma$ [18]. Expanding γ as $\gamma_0+\mathrm{Re}\,\gamma_1+\cdots$ and using the continuity of $\hat{\mathbf{n}}\cdot\mathbf{u}$ at Γ yields the inhomogeneous damped Burgers' equation

$$\gamma+\frac{d^2}{10\nu}\left[\gamma_t+\frac{9}{7}\gamma\gamma_y\right]=\hat{\mathbf{t}}\cdot\Delta\mathbf{u}_0|_\Gamma. \qquad (2)$$

In general, the right-hand side of Eq. (2) is a function of the interface shape. For simplicity, consider a nearly straight interface between two fluids with density difference $\Delta\rho$ that varies linearly with vertical position y. Then the right-hand side of Eq. (2) is proportional to $\Delta\rho(y)g$, which we write as $K-\alpha y$. The nonlinearity is responsible for steepening the vorticity, while the standard contribution arising from Darcy's law (first term on the left-hand side) is responsible for damping it. The competing effects in the damped version of Burgers' equation allow shocks to occur only under suitable initial conditions. Solving Eq. (2) by the method of characteristics [19], shocks occur if

$$\frac{d}{U}\gamma_y<-\frac{35}{9}(1+\sqrt{1-4\alpha})\frac{1}{\mathrm{Re}}. \qquad (3)$$

This result shows that a singularity will occur more readily for larger Reynolds numbers and will not occur in the strict limit of Darcy's law.

For thin fluid layers, such as the jet itself or the conduit, the dynamics of γ can be incorporated into an equation of motion of the interface(s) [20]. For two interfaces whose displacements are reflection-symmetric about a midline (as in Fig. 2), one obtains a lubrication-type equation which at leading order in h is $h_t=-(h\gamma)_y$. As discussed by Pugh and Shelley [14], given suitable initial conditions, these coupled partial differential equations can display an unbounded finite-time singularity for h or can simply relax to a traveling wave with constant γ. This is consistent with the observations shown in Fig. 2, even though the unstable growth mode is not truly unbounded. This discrepancy stems from the limited domain of validity of the lubrication approximation.

For meandering displacements the leading-order interfacial equation of motion describes a wave, $h_t=-\gamma h_y$, and as such does not have the flux form of the reflection-symmetric case. Here, the singularity in γ is inherited directly by h, which will become multivalued at a finite time. This is consistent with the overturning in Fig. 3.

We have presented a number of experimental observations concerning the rich dynamics of decelerated jets at finite Reynolds number, as well as a theoretical scenario which should serve as a starting point for a more rigorous understanding of the phenomena in Hele-Shaw flow, as well as providing general mechanisms that hold in three dimensions [13]. Among the important open problems are a detailed understanding of the conduit formation and its nonlinear interaction with the buckled jet.

[1] D. Bensimon, L. Kadanoff, S. Liang, B. Shraiman, and C. Tang, Rev. Mod. Phys. **58**, 977 (1986).

[2] E. Flekkoy, T. Rage, U. Oxaal, and J. Feder, Phys. Rev. Lett. **77**, 4170 (1996).

[3] P. Gondret and M. Rabaud, Phys. Fluids **9**, 3267 (1997).

[4] C. Ruyer-Quil, C. R. Acad. Sci., Ser. IIb: Mec., Phys., Chim., Astron. **329**, 337 (2001).

[5] F. Plouraboué and E. Hinch, Phys. Fluids **14**, 922 (2002).

[6] G. Taylor, in *Proceedings of the 12th International Congress on Applied Mechanics, Stanford, 1968*, p. 382.

[7] B. Tchavdarov, A. Yarin, and S. Radev, J. Fluid Mech. **253**, 593 (1993).

[8] L. Mahadevan, W. Ryu, and A. Samuel, Nature (London) **392**, 140 (1998).

[9] K. Helfrich and J. Whitehead, Geophys. Astrophys. Fluid Dyn. **51**, 35 (1990).

[10] M. Hanasz and H. Sol, Astron. Astrophys. **315**, 355 (1996).

[11] J. Kessler, J. Fluid Mech. **173**, 199 (1986).

[12] J. Lister, J. Fluid Mech. **175**, 413 (1987).

[13] C. Dombrowski *et al.* (unpublished).

[14] M. Pugh and M. Shelley, Commun. Pure Appl. Math. **51**, 733 (1998).

[15] Schlieren system: two 152.5-mm f/8 parabolic mirrors (Edmund Sci.); Hamamatsu C7300 digitial CCD with a 80–200 mm lens, under Labview control.

[16] *CRC Handbook of Chemistry and Physics*, edited by R. Weast (CRC Press, Boca Raton, 1979).

[17] T. Faber, *Fluid Dynamics for Physicists* (Cambridge University Press, Cambridge, 1995).

[18] G. Tryggvason and H. Aref, J. Fluid Mech. **136**, 1 (1983).

[19] G. Witham, *Linear and Nonlinear Waves* (Wiley-Interscience, New York, 1974).

[20] R. Goldstein, A. Pesci, and M. Shelley, Phys. Fluids **10**, 2701 (1998).